Numerical Study of the Ripple Resonance Diffusion of Alpha Particles in Tokamaks

Hideyuki MIMATA, Keiji TANI[1)], Hiroaki TSUTSUI, Kenji TOBITA[2)], Shunji TSUJI-IIO and Ryuichi SHIMADA

Tokyo Institute of Technology, Tokyo 152-8550, Japan
[1)]*Nippon Advanced Technology Co., Ltd. Naka Office, Naka 311-0193, Japan*
[2)]*Japan Atomic Energy Agency, Naka 311-0193, Japan*

(Received 30 September 2008 / Accepted 16 January 2009)

The energy dependence of the diffusion coefficients of α particles in rippled fields of tokamaks is numerically investigated with an orbit-following Monte Carlo code. The diffusion coefficients are enhanced around the ripple resonance energy while they are not so much enhanced in the neighborhood of it. Consequently, they have a local minimum near the resonance energy, and hence they have an M-shaped energy dependence. Ripple resonance is caused by a radial change of the toroidal precession of banana particles, and creates islands in $(N\phi, \psi)$ phase space. Since particles outside the separatrix are the main contributors to diffusion enhancement, the M-shaped energy dependence is explained by the co-existence of open and closed orbits in the phase space. Ripple resonance diffusion is dominant for fusion-produced α particles since the resonance energy width occupies a large portion of the energy range in their slowing-down processes.

Keywords: α particle, tokamak, particle diffusion, ripple resonance, mapping model, Poincaré map

DOI: 10.1585/pfr.4.008

1. Introduction

The confinement of fusion-produced α particles is important to maintain burning plasmas in tokamaks. Although α particles are well confined in axisymmetric fields, it has been shown that the loss of α particles due to magnetic field ripple caused by discrete toroidal field (TF) coils is dominant in the diffusion process in actual tokamaks, with orbit-following Monte Carlo (OFMC) simulations [1, 2]. However, the understanding of the loss processes in detail is inadequate.

Banana particles contribute significantly to the loss. Since radial displacement by toroidal drift depends on the toroidal phase $N\phi$ of a banana tip between TF coils [3]; the change in the phase due to both toroidal precession and Coulomb collisions is important. In a low energy range of $\tau_{\rm eff} < \tau_{\rm b}$, where $\tau_{\rm eff}$ is the effective collision time in which $N\phi$ is changed by about π and $\tau_{\rm b}$ is the bounce time of banana motion, diffusion coefficients do not depend on collision frequency (ripple plateau diffusion) [4].

In a high energy range, the Larmor radius is so large that radial displacement due to ripples exceeds a certain threshold; then collisionless orbits become ergodic and particles are rapidly lost from the plasma [5]. Ripple plateau diffusion is dominant after α particles are sufficiently slowed, while the ergodic loss is dominant only for high energy particles at the plasma edge where ripples are large. Since α particles are mostly produced in the core of the plasma, ergodic loss is not so important. The pitch-angle scattering of fusion-produced α particles in one bounce motion is small enough to maintain banana orbits. Thus, collisonless orbits are important for the diffusion process. Since the radial displacement of a banana orbit by ripples depends on the toroidal phase at the banana tip [3], the cumulated radial displacement becomes resonantly large when the difference in the toroidal angles of successive banana tips is a multiple of the toroidal angle of adjacent TF coils (ripple resonance). This toroidal distance of successive banana tips is determined by toroidal precession. Yushmanov theoretically analyzed this ripple resonance diffusion by means of the banana-drift kinetic equation without radial change in toroidal precession because it is much less than that of the toroidal length of the banana orbit [6]. Since the toroidal precession, however, strongly depends on radial position in an actual tokamak, we investigated ripple resonance diffusion in a realistic system with radial change in toroidal precession by numerical calculations based on an OFMC simulation.

In Sec. 2, the calculation model is briefly explained, and the energy dependence of the diffusion coefficients is shown in Sec. 3. Section 4 describes the collisionless orbit of an α particle in rippled fields to explain the energy dependence of the diffusion coefficients calculated in Sec. 3, and the discussion is presented in Sec. 5. The conclusions are given in Sec. 6.

author's e-mail: hmimata@nr.titech.ac.jp

2. Calculation Model

In this paper, the orbit of an α particle is numerically evaluated with the following guiding center equations,

$$m\frac{\mathrm{d}v_\parallel}{\mathrm{d}t} = -\mu_\mathrm{m}\frac{(\boldsymbol{B}\cdot\boldsymbol{\nabla})B}{B}, \tag{1}$$

$$\boldsymbol{v}_\perp = \frac{\mu_\mathrm{m} + mv_\parallel^2/B}{eB^2}(\boldsymbol{B}\times\boldsymbol{\nabla}B), \tag{2}$$

in the same way as the OFMC code [1, 2], where $\boldsymbol{B}$ is the magnetic field, μ_m is the magnetic moment, $v_\parallel$ and $v_\perp$ are the velocity parallel and perpendicular to the magnetic field, B is the magnetic field strength, and m, e are the mass and electric charge of α particles, respectively. In an axisymmetric vacuum toroidal field, guiding center equations (1), (2) conserve the toroidal canonical momentum $P_\phi = mRv_\phi + e\psi$, where R, v_ϕ and ψ are the major radius, the toroidal component of velocity and the poloidal magnetic flux, respectively. The velocities of α particles are also changed by Coulomb collisions with a bulk plasma in the directions parallel and perpendicular to the velocity, $\mathrm{d}v_\mathrm{L}/\mathrm{d}t$, $\mathrm{d}v_\mathrm{T}/\mathrm{d}t$. Then the velocity of α particles changes according to both the guiding center equations (1), (2) and Coulomb collisions,

$$\frac{\mathrm{d}v_\parallel}{\mathrm{d}t} = \frac{\mathrm{d}v_\mathrm{L}}{\mathrm{d}t}\frac{v_\parallel}{v} - \frac{\mathrm{d}v_\mathrm{T}}{\mathrm{d}t}\frac{v_\perp}{v}\sin\xi, \tag{3}$$

$$\left(\frac{\mathrm{d}v_\perp}{\mathrm{d}t}\right)^2 = \left[\left(v + \frac{\mathrm{d}v_\mathrm{L}}{\mathrm{d}t}\right)^2 + \left(\frac{\mathrm{d}v_\mathrm{T}}{\mathrm{d}t}\right)^2 - \left(v_\parallel + \frac{\mathrm{d}v_\parallel}{\mathrm{d}t}\right)^2\right] - v_\perp^2. \tag{4}$$

The Larmor phase, ξ, is given by a uniform random number between zero and 2π, and the time evolution of v_L and v_T are given by a Monte Carlo method satisfying the Gaussian process,

$$\frac{\mathrm{d}\langle v_\mathrm{L}\rangle}{\mathrm{d}t} = -\frac{v}{\tau_\mathrm{s}}, \tag{5}$$

$$\frac{\mathrm{d}\langle v_\mathrm{T}\rangle}{\mathrm{d}t} = 0, \tag{6}$$

$$\frac{\mathrm{d}\left\langle(v_\mathrm{L} - \langle v_\mathrm{L}\rangle)^2\right\rangle}{\mathrm{d}t} = -\frac{v^2}{4\tau_\varepsilon}, \tag{7}$$

$$\frac{\mathrm{d}\left\langle(v_\mathrm{T} - \langle v_\mathrm{T}\rangle)^2\right\rangle}{\mathrm{d}t} = -\frac{v^2}{\tau_\mathrm{d}}, \tag{8}$$

where $\langle\rangle$ denotes emsemble average, τ_s is the slowing-down time, τ_d is the deflection time, and τ_ε is the energy-exchange time [7, 8]. Diffusion coefficients are evaluated by the rate of change in a variance of the toroidal canonical momentum, which corresponds to the poloidal magnetic flux at a banana tip, $P_\phi = mRv_\phi + e\psi = e\psi_\mathrm{b}$,

$$D = \frac{1}{2}\frac{\mathrm{d}}{\mathrm{d}t}\left\langle(P_\phi - \left\langle P_\phi\right\rangle)^2\right\rangle \Big/ \left(e\frac{\mathrm{d}\psi}{\mathrm{d}\rho}\right)^2. \tag{9}$$

3. Numerical Results of Ripple Diffusion

The diffusion coefficients of α particles are calculated in rippled fields using the calculation model given in Sec. 2. The dependence of the diffusion coefficients on energy, ripple strength, and other parameters is calculated with test particles launched from the same banana tip position. The calculation parameters are summarized in Table 1. For a qualitative understanding of ripple resonance, we chose an equilibrium with a circular plasma cross section with major radius $R_0 = 6$ m and minor radius $a = 2$ m, since diffusion phenomena in tokamak plasmas with circular cross sections are well understood. The toroidal magnetic field is given by $B_\phi = (B_0R_0/R)(1 + \gamma(R,Z)\cos N\phi)$ where N is the number of TF coils and the ripple strength $\gamma(R,Z)$ is a function of the poloidal coordinate (R,Z). The safety factor, $q(\rho)$, and the axisymmetric poloidal magnetic flux, $\psi(\rho)$, are given as functions of the minor radius of the magnetic surfaces as shown in Fig. 1. The figure shows that the ripple strength becomes large in the plasma periphery. Thus we chose $T = 3$ keV as the plasma periphery temperature in this work. All α particles with same initial kinetic energy, W, and magnetic moment, μ_m, start from banana tips on the same magnetic surface, while toroidal angles are randomly given. Because the magnetic field is rippled, the initial poloidal angle of each test particle is changed so that the magnetic moment becomes the initial set value.

Table 1 Calculation parameters

major radius	$R_0 = 6$ m
minor radius	$a = 2$ m
toroidal field	$B_0 = 3.0$ T
safety factor $q(\rho = a)$	$q_a = 4.1$
number of TF coils	$N = 18$
ripple resonance energies	0.4, 1.5, 2.9, 4.4 MeV
plasma density	$n_\mathrm{DT} = 10^{20}$ m^{-3} (spatially uniform)
plasma temperature	$T = 3$ keV (spatially uniform)
characteristic times of α particles at 1.5 MeV	
bounce time	$\tau_\mathrm{b} \sim 4.2\times10^{-5}$ s
slowing down time	$\tau_\mathrm{s} \sim 6.5\times10^{-2}$ s
deflection time	$\tau_\mathrm{d} \sim 3.0$ s
energy-exchange time	$\tau_\varepsilon \sim 7.7$ s

Figure 2 (red line) shows the energy dependence of diffusion coefficients in rippled fields. The diffusion coefficients in the axisymmetric field (black dotted line), which agree with neoclassical diffusion coefficients ($\propto W^{-1/2}$), are also shown. The radial displacement by the ripple depends on the toroidal phase of the banana tip [3]. Generally, this radial displacement is canceled during several bounces because the toroidal phase of every banana tip varies. However, when the toroidal angle difference between successive banana tips equals a multiple of the toroidal angle between adjacent TF coils, it maintains the same radial displacement at every banana tip and its cumu-

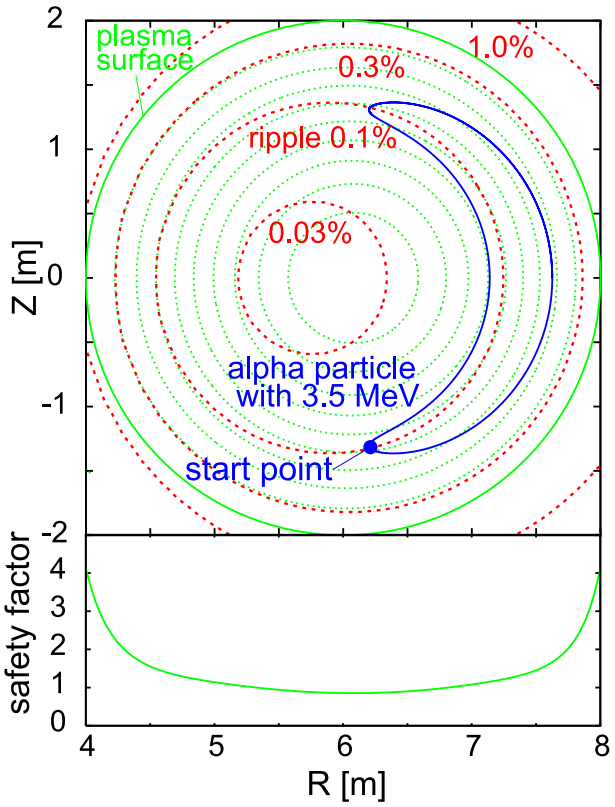

Fig. 1 An equilibrium configuration and the distribution of ripple amplitude and safety factor used in the calculation of diffusion coefficients. All particles start from the same banana tip position indicated in the figure.

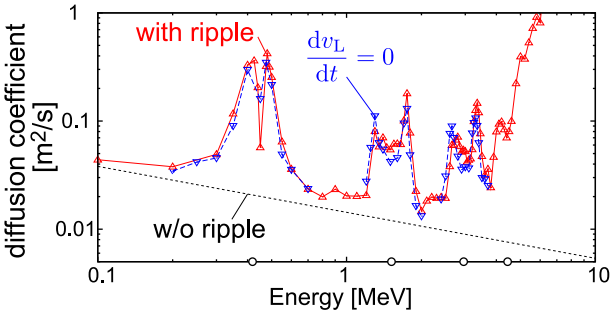

Fig. 2 Energy dependence of the diffusion coefficient in rippled fields. In the magnetic configuration shown in Fig. 1, the ripple resonance energies without ripples are 0.4, 1.5, 2.9, and 4.4 MeV, indicated by open circles on the abscissa. Particles start from the same banana tip at any energy.

lative radial displacement becomes large because of resonance (ripple resonance). This ripple resonance condition depends on the energy of an α particle. In the magnetic configuration used in this paper, ripple resonance energies are 0.4, 1.5, 2.9, and 4.4 MeV.

In previous research [6], the diffusion coefficients in rippled fields have maxima at the resonance energies be-

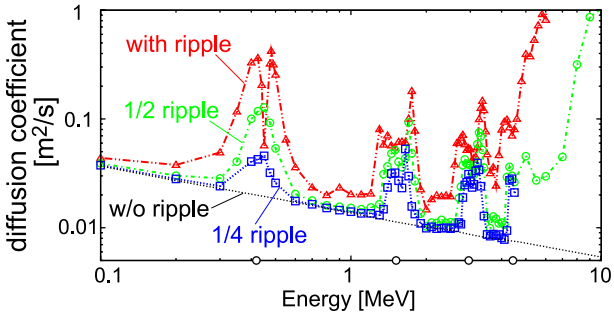

Fig. 3 The energy dependence of diffusion coefficients changes with the ripple strength. The open circles on the abscissa indicate ripple resonance energies without ripples.

cause α particles resonate with ripples. In our calculation, however, the diffusion coefficients have an M-shaped energy dependence; local maxima on both sides of the resonance enery and a local minimum near the resonance energy.

The blue dashed lines in Fig. 2 are the diffusion coefficients without slowing from collisions. Figure 2 shows that the difference in diffusion coefficients with and without the effect of the slowing down is very small, and hence the diffusion was found to be caused mainly by pitch angle scatterings. Concerning the symmetry of the M-shape, the diffusion coefficients with the slowing-down effect have larger values on the higher-energy side. This implies that resonant particles are partly provided from the higher-energy side through slowing-down processes. The diffusion coefficient also changes with the ripple strength and plasma density. The value of the coefficients is proportional to the ripple strength, while the energy range where diffusion is enhanced by the ripple widen with increasing ripple strength as shown in Fig. 3. Diffusion coefficients are roughly proportional to the plasma density (proportional to the collision frequency) in a resonance range (1.5 MeV) and in a non-resonance range (1.0 MeV), as shown in Fig. 4. The results in Figs. 3 and 4 demonstrate that the characteristic time of the diffusion process is proportional to the collision frequency and the characteristic step size depends on the ripple strength.

Since the diffusion coefficients are large around resonance energies, resonant particles enhance the diffusion. Moreover, the diffusion coefficients do not peak at the resonance energy but show an M-shaped dependence around the resonance energy. Also, the ripple strength not only enhances the diffusion coefficients but also changes the energy dependence near the resonance point. Because the ripple resonance of fast ions is a collisionless phenomenon, collisionless orbits play an important role in the diffusion process in this energy range. In the next section we investigate collisionless orbits in rippled fields to understand the M-shaped dependence of diffusion coefficients.

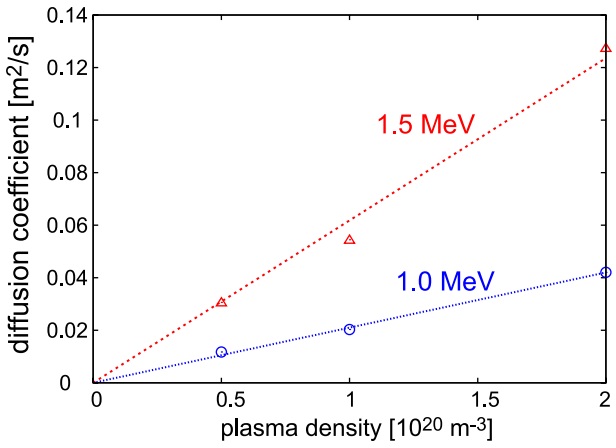

Fig. 4 The dependence of diffusion coefficients on the plasma density, which is roughly proportional to the collision frequency, at resonance (1.5 MeV) and nonresonance (1.0 MeV) energies.

4. Collisionless Orbits of Ripple Resonance Particles

In this section, we describe the behavior of banana particles without collisions in rippled fields. The toroidal canonical momentum,

$$P_\phi = mv_\parallel \frac{I}{B} + e\psi = e\psi_\mathrm{b}, \tag{10}$$

where $v_\parallel$ is the velocity parallel to the magnetic field and $I = RB_\phi$, is conserved in axisymmetric fields and corresponds to the poloidal magnetic flux at the banana tip, ψ_b. However it is not conserved in rippled fields and has displacements located mainly near banana tips [3, 5, 9, 10],

$$\Delta\psi = \Delta_\mathrm{b} \sin(N\phi \mp \pi/4), \tag{11}$$

$$\Delta_\mathrm{b} = I\gamma\rho_\mathrm{L}\sqrt{\left|\frac{\pi Nq}{(\partial B(\rho,\theta,\phi)/\partial\theta)/B}\right|}, \tag{12}$$

where ρ_L is the Larmor radius, $\mp$ corresponds to the upper and lower banana tip, and each parameter is evaluated at the banana tip. Since this displacement mainly occurs only near banana tips, the banana motion is described approximately by a mapping method that follows only the banana tips. During one half-bounce, the change in the toroidal phase at the banana tip in axisymmetric fields is given by

$$\Delta\phi = \phi_\mathrm{p} \pm \phi_\mathrm{b}. \tag{13}$$

Here ϕ_b, ϕ_p are described in Ref. [9],

$$\phi_\mathrm{b} = 2q\theta_\mathrm{b}, \tag{14}$$

$$\phi_\mathrm{p} = \frac{\sqrt{2}q^2}{\varepsilon^{3/2}}\frac{\sqrt{2mW}}{eBR}\left(1-\frac{\sin^2\zeta}{2}\right)\left[E(\Theta)-\frac{K(\Theta)}{2}\right.$$
$$\left.+2S\left(E(\Theta)-K(\Theta)\cos^2\frac{\theta_\mathrm{b}}{2}\right)\right], \tag{15}$$

where W is the energy of the particle, $E(\Theta)$, $K(\Theta)$ are the complete elliptic integrals, $S = (\rho/q)(\mathrm{d}q/\mathrm{d}\rho)$, $\Theta = \sin(\theta_\mathrm{b}/2)$, $\varepsilon = r/R$, and $\sin\zeta = v_\perp/v$. Since energy is conserved in collisionless processes, ϕ_b and ϕ_p are functions of the poloidal magnetic flux, $\phi_\mathrm{b} = \phi_\mathrm{b}(\psi)$, $\phi_\mathrm{p} = \phi_\mathrm{p}(\psi)$. Thus, starting from the lower banana tip, (ϕ_i^-, ψ_i^-), successive bounce points are given by the banana tip map [5, 10],

$$\psi_i^+ = \psi_i^- + \Delta_\mathrm{b}\sin(N\phi_i^- + \pi/4), \tag{16}$$
$$\phi_i^+ = \phi_i^- + \phi_\mathrm{b}(\psi_i^+) + \phi_\mathrm{p}(\psi_i^+), \tag{17}$$
$$\psi_{i+1}^- = \psi_i^+ + \Delta_\mathrm{b}\sin(N\phi_i^+ - \pi/4), \tag{18}$$
$$\phi_{i+1}^- = \phi_i^+ - \phi_\mathrm{b}(\psi_{i+1}^-) + \phi_\mathrm{p}(\psi_{i+1}^-). \tag{19}$$

The total change in the position of the lower banana tip in one bounce is given by

$$\psi_{i+1} = \psi_i + 2\Delta_\mathrm{b}\sin(N\phi_i + \Phi)\cos(\Phi - \pi/4), \tag{20}$$
$$\phi_{i+1} = \phi_i + 2\phi_\mathrm{p}(\psi_{i+1}), \tag{21}$$

ignoring corrections to ψ of order Δ_b^2 and ϕ of order Δ_b where $\Phi = N\left(\phi_\mathrm{b}(\psi) + \phi_\mathrm{p}(\psi)\right)/2$. Thus the ripple resonance condition, in which the toroidal phase, $N\phi$ of the particle is constant, is given by

$$2N\phi_\mathrm{p} = 2k\pi \tag{22}$$

for all integers k. Furthermore, particles that satisfy Eq. (22) and

$$2N\phi = (2l-k)\pi - N\phi_\mathrm{b} \tag{23}$$

for all integers l are fixed in the phase space, $(N\phi, \psi)$.

To analyze the Poincaré map of Eqs. (20) and (21), we replace the discrete points of the map with continuous curves by introducing the differential time variable $\mathrm{d}t$ with time measured in units of one bounce. Assuming ϕ_b and ϕ_p as linear functions of ψ near the resonance surface $\psi = \psi_k$ $(2N\phi_\mathrm{p}(\psi_k) = 2k\pi)$, Eqs. (20) and (21) are converted to the differential equations

$$\mathrm{d}\psi = 2\Delta_\mathrm{b}\sin(N\phi + \Phi)\cos(\Phi - \pi/4)\mathrm{d}t, \tag{24}$$
$$\mathrm{d}\phi = 2\phi'_{\mathrm{p}k}(\psi - \psi_k)\mathrm{d}t, \tag{25}$$

where $'$ represents $\partial/\partial\psi$. If $\Phi = \Phi_k(\Phi_k = \Phi(\psi_k))$, these differential equations are solved,

$$\psi = \psi_k \pm \sqrt{\frac{2\Delta_\mathrm{b}}{N\phi'_\mathrm{p}}\cos(\Phi_k - \pi/4)\left[C - \cos(N\phi + \Phi_k)\right]}, \tag{26}$$

where C is the integration constant. Figure 5 compares Poincaré maps using the guiding center equations (1) and (2), the mapping model (16)-(19), and the analytic representation of Eq. (26). Representation (26) is a good approximation to the guiding center solutions. Near the resonance energy, an island structure formes around the resonance surface, $\psi = \psi_k$. When $-1 < C < 1$, the corresponding orbit is located inside the separatrix. As shown in Fig. 5, the fixed point satisfying Eqs. (22) and (23) is the O-point or X-point determined by the sign of $\cos(\Phi_k - \pi/4)/(N\phi'_\mathrm{p})$. Although this island structure is determined by ψ_k, Φ_k, and $\Delta_\mathrm{b}/N\phi'_\mathrm{p}$ as expressed in Eq. (26);

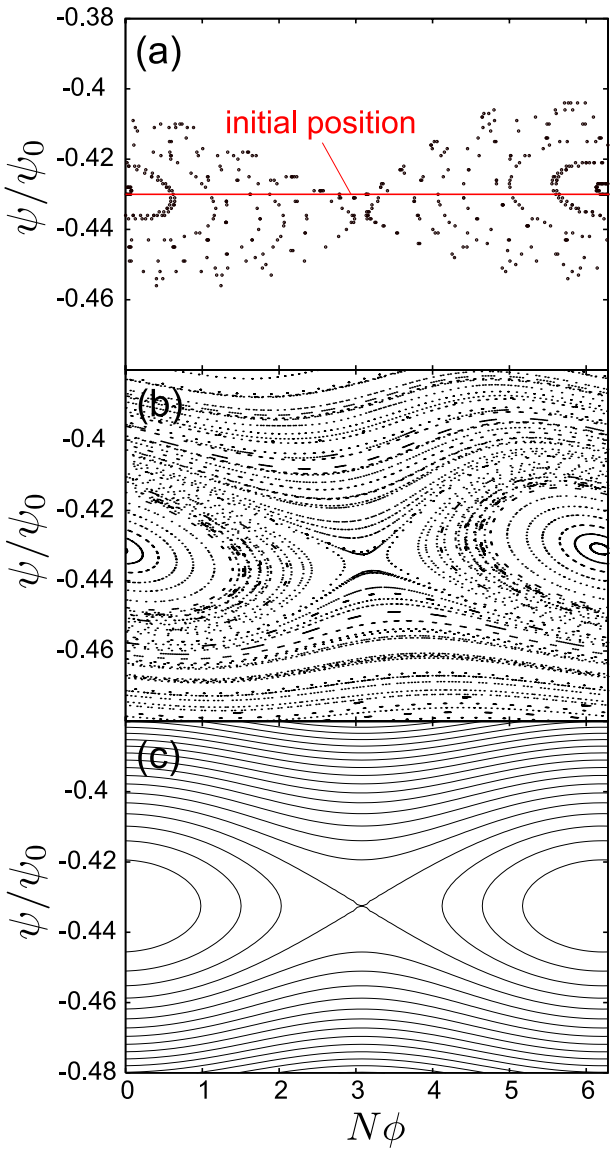

Fig. 5 Comparison of Poincaré plot of orbits calculated with the guiding center equations, the mapping of Eqs. (16)-(19), and the analytical representation of Eq. (26) at 1.5 MeV. ψ_0 is the difference in the poloidal magnetic flux between the plasma surface and magnetic axis, and $\psi/\psi_0 = 0$ and -1 correspond to the plasma surface and magnetic axis, respectively. The starting positions of test particles for Fig. 2 is on the red line; the initial collisionless orbits are those that cross the red line.

the energy dependence of the structure mainly depends on ψ_k and Φ_k because of the energy dependences of $\Delta_b \propto W^{1/2}$ and $\phi_p \propto W^{1/2}$. The structure of collisionless orbits around the resonance energy is, therefore, determined by these two parameters as follows: the position of the O-point is determined by ψ_k and Φ_k, while the width of the island is determined by Φ_k.

The distribution of α particles in the phase space is specified by the structure of orbits and the initial positions. When test particles initially satisfy the resonance condition $\psi = \psi_k$, they are localized in the separatrix, as shown in Fig. 5 (a). When the energy decreases under the fixed banana tip condition, ψ_k increases in the magnetic configuration used in this paper. Hence, the fixed initial surface, ψ = const., is located on the lower side of the resonance surface $\psi = \psi_k$, and the particles also exist in both inside and below the separatrix. The percentage of particles located outside of the separatrix increases with the difference between the particle and resonance energies. If the energy of the α particle is far from the resonance energy, the particles in the island disappear, while the island structure does not disappear in the phase space. Here, introducing

$$H(N\phi,\psi) \equiv N\phi'_p(\psi-\psi_k)^2 + 2\Delta_b\cos(N\phi+\Phi_k)\cos(\Phi_k-\pi/4), \quad (27)$$

this is a constant of motion and the Hamiltonian of Eqs. (24) and (25). The relationship between H and the integration constant C can be expressed as follows;

$$C = \frac{H}{2\Delta_b\cos(\Phi_k-\pi/4)}. \quad (28)$$

Therefore, the collisionless orbit of each test banana particle can be specified by C = const. ($\Leftrightarrow$ H = const.) and orbits do not cross each other in the phase space, $(N\phi,\psi)$. As example values are given in Table 1, the characteristic times based on the collision are long enough compared to the bounce time. Thus, we can consider the following diffusion processes in the phase space:

1. orbits, on which particles initially exist, are determined by the initial condition,
2. particles are uniformly distributed on each orbit, and
3. diffusion is represented as the change in Hamiltonian H ($\Leftrightarrow$ C), which is caused through the change in constants ψ_k and Φ_k by collisions.

According to the model, a discontinuous jump of ψ and enhanced diffusion occur when a particle outside the separatrix enters the island by collisions. Therefore diffusion is expected to be determined by both the co-existence of open and closed collisionless orbits and the initial distribution of the test particles in the phase space.

5. Ripple Resonance Diffusion and its Energy Dependence

In a collisionless case, although particles spread in the phase space, they maintain periodic motion on their collisionless orbits where C evaluated by Eq. (28) is const., and diffusion does not occur. Collisions change C with time according to changes in ψ_k and Φ_k, causing diffusion. Since particles spread along an orbit, C = const., in much shorter time than the collision time as described in Sec. 4, we evaluated the diffusion coefficients of each orbit labeled by C = const. Initial positions of test particles were randomly distributed on each collisionless orbit. In collisionless cases, although C in the analytic representation (26) is

constant, C obtained from the guiding center orbit is not constant. Hence, we introduce a label for each orbit, $\tilde{C}$, defined by

$$\tilde{C} = \left(\frac{\psi - \psi_k}{\tilde{\Delta}_p}\right)^2 - 1 = \frac{H(\pi - \Phi_k, \psi_k)}{2\Delta_b \cos(\Phi_k - \pi/4)}, \qquad (29)$$

where $2\sqrt{2}\tilde{\Delta}_p$ is the width of the island skimmed from the Poincaré map of the guiding center orbits. The results are shown in Fig. 6 (A). At $\tilde{C} > 1$, there are two plots corresponding to the upper and the lower side of the island. The Poincare plot of orbits of particles with a fixed energy of 1.5 MeV is shown in Fig. 6 (B). The diffusion coefficients are large just outside the separatrix and become smaller with the distance from the separatrix. On the other hand, the diffusion coefficients inside the separatrix are small. This behavior can be interpreted as follows; When particles outside the separatrix enter the separatrix by collisions, the averaged radial positions jump by about one-half of the island width and hence diffusion is enhanced. Away from the island ($\tilde{C}$ becomes large), the time for particles to reach the separatrix by collisions becomes longer, and diffusion becomes smaller. Even if a particle inside the separatrix leaves it because of collisions, the averaged radial positions do not vary much, since the particles get to both sides of the island with nearly equal probabilities. Consequently, the diffusion coefficients inside the separatrix are small.

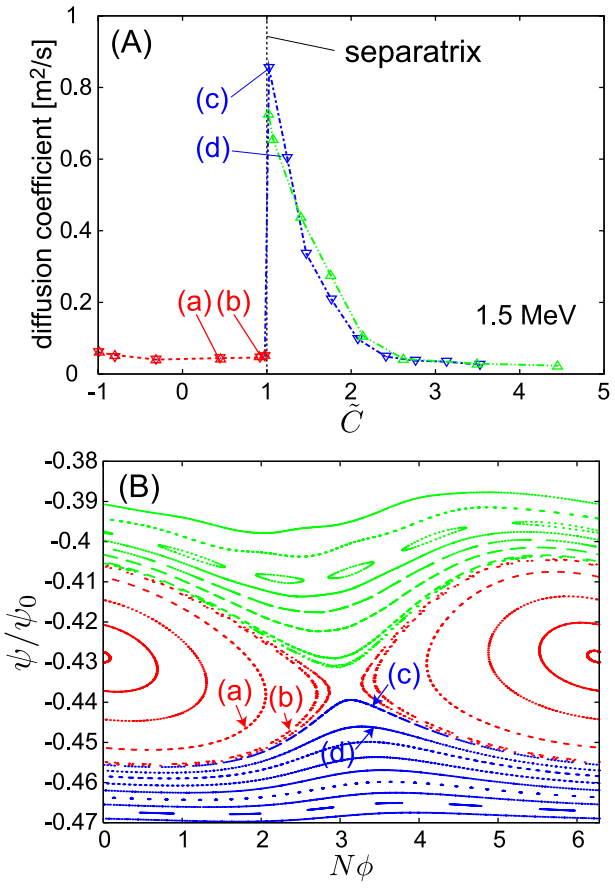

Fig. 6 (A) $\tilde{C}$-dependence of diffusion coefficients at 1.5 MeV. $\tilde{C} > 1$, two plots correspond to orbit on the upper and lower side of the island. (a)-(d) correspond to the initial orbits in (B). (B) Initial orbits of the calculation of each diffusion coefficient in (A). Initial positions are randomly given from a few hundred bounce motions on these collisionless orbits.

When the energy and magnetic moment of particles vary because of collisions, the structure of the Poincaré map changes. Thus, diffusion is caused not only by the transition of orbits in Fig. 6 (B), but also by the change in the structure of the Poincaré map. Even in that case, diffusion coefficients have a maxima just outside of the $\tilde{C} = 1$ surface, because the separatrix is always on $\tilde{C} = 1$

Figure 7 shows the time evolution of $\left\langle (P_\phi - \left\langle P_\phi \right\rangle)^2 \right\rangle$ of particles initially in orbits (b) and (c) in Fig. 6. Since the oscillations in Case (b) are due to the time in which particles go around the island, diffusion coefficients are evaluated for a time period longer than this as indicated by the straight line. The initial large value in Case (b) is due to spreading along the island. The slope is not large because $\left\langle P_\phi \right\rangle$ does not vary much even if particles leave the separatrix by collisions. On the other hand, the initial value in Case (c) is small. Its subsequent rise, which was confirmed to follow the Gaussian process, becomes steep because of stepwise changes in $\left\langle P_\phi \right\rangle$ of particles that enter the separatrix by collisions. After that, once particles are spread along the island, its slope becomes small. For comparison, those time evolutions in collisionless cases are also shown in Fig. 7.

Next, we investigate the relationship between the diffusion coefficients of Figs. 2 and 6. The green bars in Fig. 8 denote the range of initial $\tilde{C}$, which was evaluated from Eq. (29) using the initial orbits in the Poincaré map, at each energy. The blue line in Fig. 8 shows the diffusion coefficients calculated from the $\tilde{C}$-dependence of diffusion co-

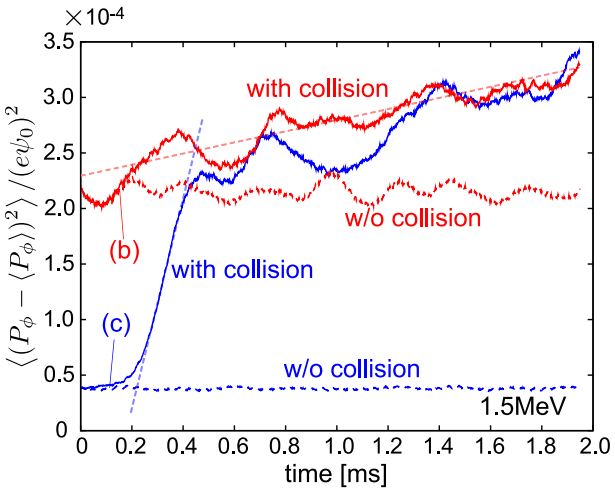

Fig. 7 Time evolutions of $\left\langle (P_\phi - \left\langle P_\phi \right\rangle)^2 \right\rangle$ (collisional and collisionless case) starting from orbits located at inner (b) and outer (c) sides of the separatrix in Fig. 6.

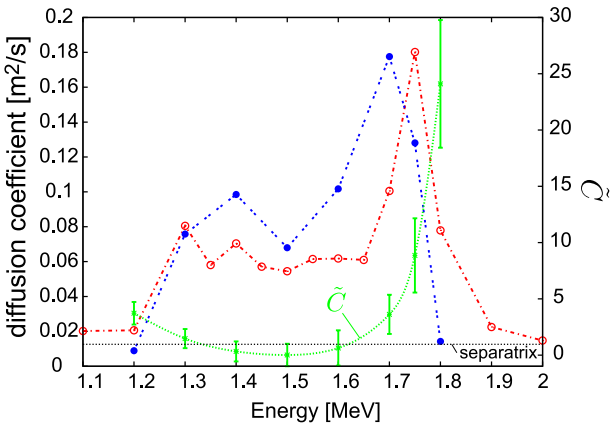

Fig. 8 Diffusion coefficients (dotted blue line) evaluated from $\tilde{C}$-dependence of the diffusion coefficient at each energy. Red line is the energy dependence of the diffusion coefficients shown in Fig. 2. Green bar is the initial range of $\tilde{C}$ in Fig. 2, and the blue line is obtained by integrating the $\tilde{C}$-dependence of diffusion coefficients over this range.

efficients. At each energy, it was evaluated by integrating the diffusion coefficients depending on $\tilde{C}$ over the initial distribution of orbits, $\tilde{C}$ (green bars). Almost the same energy dependence as shown in Fig. 2 was reproduced. Three Poincaré maps at three energies are plotted in Fig. 9. The diffusion coefficients are small near the resonance energy because many particles are inside the separatrix and do not enhance the diffusion to a great extent. On the other hand, the diffusion coefficients are large at both sides of the resonance energy because substantial open orbits outside of the separatrix supply particles that jump into the island by collisions, enhancing diffusion. Thus the M-shaped dependence on the energy has been elucidated. This M-shaped dependence does not appear in Yushmanov's work [6] because of the neglect of the radial change in ϕ_p, although this radial change creates the island structure, which contributes to the ripple diffusion.

Finally, we investigated the energy width of the M-shaped ripple resonance diffusion. The diffusion coefficient becomes large when test particles exist outside the separatrix in the phase space. We evaluated the energy range where the separatrix intersects the straight line ψ = const., which represents the initial positions of test particles. Rewriting Eq. (26) as

$$\psi = \psi_k \pm \Delta_p \sqrt{C - \cos(N\phi + \Phi_k)}, \tag{30}$$

$$\Delta_p = \sqrt{\left|\frac{2\Delta_b}{N\phi'_p}\cos(\Phi_k - \pi/4)\right|}, \tag{31}$$

the condition that the initial positions overlap the separatrix is

$$|\psi - \psi_k| \le \sqrt{2}\Delta_p. \tag{32}$$

If ψ at a banana tip is fixed, the resonance surface ψ_k changes according to the particle energy. When the energy changes from W_k to $W_k + \Delta W$, the resonance surface changes as

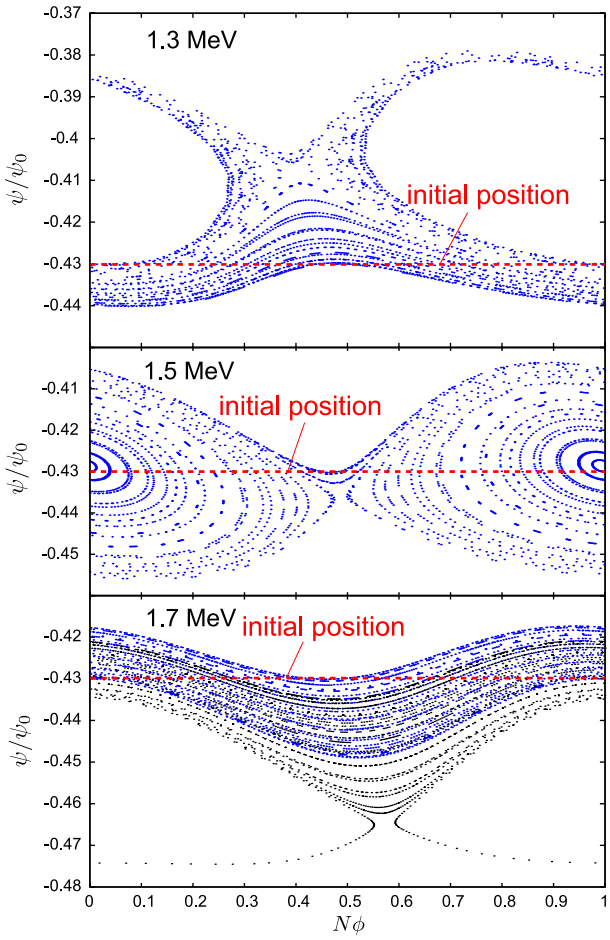

Fig. 9 Changes of collisionless orbits (dotted blue lines) that start from ψ = const. (dotted red lines) on the Poincaé map depending on energy. At resonance energy (1.5 MeV), many particles are inside the separatrix. On the other hand, at both sides of the resonance energy many particles are outside of the separatrix.

$$\psi_k(W) = \psi_k(W_k) + \frac{\partial\psi_k}{\partial W}\Delta W, \tag{33}$$

where W_k is the kth resonance energy at a certain banana tip ψ and $\psi_k(W_k) = \psi$. Then if

$$\left|\frac{\partial\psi_k}{\partial W}\Delta W\right| \le \sqrt{2}\Delta_p, \tag{34}$$

the initial orbit overlaps the separatrix and the resonance width is

$$|\Delta W| \le \sqrt{2}\Delta_p\left|\frac{\phi'_p}{\partial\phi_p/\partial W}\right|. \tag{35}$$

Since $\partial\phi_p/\partial W = \phi_p/2W$ and $\Delta_p \propto \gamma^{1/2}$, the resonance width is proportional to W and $\gamma^{1/2}$. Substituting the value of resonance energy, 1.5 MeV, the resonance width is 0.73 MeV and closely agrees with that evaluated from

Fig. 2. As seen in Fig. 2, the resonance width occupies a substantial energy range around the theoretical resonance energy. In the present work, the ripple resonance diffusion of banana particles with a specific pitch angle was investigated. Note that all banana particles can basically resonate with the TF ripples as they slow down. Hence, ripple resonance dominates the transport process of α particles in their slowing-down process.

6. Conclusions

The energy dependences of the diffusion coefficients of α particles in rippled fields were investigated by using an orbit-following Monte Carlo code. This work considered the effect of radial changes in the toroidal precession, which was neglected in previous work. Concluding remarks are made as follows.

1. The diffusion coefficients are enhanced around the ripple resonance energy while they are not greatly enhanced in its neighborhood of it and hence they have an M-shaped dependence on the energy.
2. The resonance width has a finite energy range proportional to W for the energy and $\gamma^{1/2}$ for the ripple strength. Ripple resonance diffusion is dominant for fusion-produced α particle, as the resonance energy width occupies a large portion of the energy range and basically all banana particles can resonate with the TF ripples as they slow down.
3. Analytical studies using a mapping method show that particles outside the separatrix are the main contributors to ripple resonance diffusion, since they can enter the separatrix by collisions and then the averaged radial position changes in a stepwise manner. Accordingly the diffusion coefficients are enhanced at both sides of the resonance energy where the percentage of particles outside of the separatrix is high, and the diffusion coefficients have an M-shaped dependence on the energy.

In these processes, radial changes in the toroidal precession were found to play a very important role. It is, therefore, clarified that the toroidal precession cannot be neglected when investigating ripple diffusion.

Acknowledgments

The authors would like to thank Dr. M. Azumi for stimulating comments. This work was carried out as a collaborative study between the Tokyo Institute of Technology and Japan Atomic Energy Agency and partially supported by the Japan Society for the Promotion of Science, Grant-in-Aid for Scientific Research (B), 17360440.

[1] K. Tani, T. Takizuka, M. Azumi and H. Kishimoto, Nucl. Fusion **23**, 657 (1983).
[2] K. Tani, T. Takizuka and M. Azumi, Nucl. Fusion **33**, 903 (1993).
[3] R.J. Goldston and H.H. Towner, J. Plasma Physics **26**, 283 (1981).
[4] A.H. Boozer, Phys. Fluids **23**, 2283 (1980).
[5] R.J. Goldston, R.B. White and A.H. Boozer, Phys. Rev. Lett. **47**, 647 (1981).
[6] P.N. Yushmanov, Nucl. Fusion **23**, 1599 (1983).
[7] K. Tani, M. Azumi, H. Kishimoto and S. Tamura, J. Phys. Soc. Jpn. **50**, 1726 (1981).
[8] B.A. Turbnikov, Rev. Plasma Phys. **1**, 105 (1965).
[9] P.N. Yushmanov, Rev. Plasma Phys. **16**, 117 (1990).
[10] R.B. White, R.J. Goldston, M.H. Redi and R.V. Budny, Phys. Plasmas **3**, 3034 (1996).